SLE description of the nodal lines of random wavefunctions

2007 J. Phys. A: Math. Theor. 40 381

(http://iopscience.iop.org/1751-8121/40/3/003)

INSTITUTE OF PHYSICS PUBLISHING JOURNAL OF PHYSICS A: MATHEMATICAL AND THEORETICAL

J. Phys. A: Math. Theor. **40** (2007) 381–395 doi:10.1088/1751-8113/40/3/003

SLE description of the nodal lines of random wavefunctions

E Bogomolny, R Dubertrand and C Schmit[1]

CNRS, Université Paris-Sud, UMR 8626, Laboratoire de Physique Théorique et Modèles Statistiques, 91405 Orsay, France

E-mail: remy.dubertrand@lptms.u-psud.fr

Received 7 September 2006, in final form 23 October 2006
Published 20 December 2006
Online at stacks.iop.org/JPhysA/40/381

Abstract

The nodal lines of random wavefunctions are investigated. We demonstrate numerically that they are well approximated by the so-called SLE_6 curves which describe the continuum limit of the percolation cluster boundaries. This result gives additional support to the recent conjecture that the nodal domains of random (and chaotic) wavefunctions in the semi-classical limit are adequately described by the critical percolation theory. It is also shown that using the dipolar variant of SLE reduces significantly finite size effects.

PACS numbers: 05.45.Mt, 03.65.Sq, 64.60.Ak

1. Introduction

In 1977 Berry conjectured [1] that the wavefunctions of chaotic quantum systems can statistically be described by Gaussian random functions with a spectrum computed from the ergodic average.

For example, the wavefunctions for two-dimensional billiards without magnetic field $\Psi(\vec{x})$ have to obey the equation

$$(\Delta + k^2)\Psi(\vec{x}) = 0 \tag{1}$$

and, say, the Dirichlet boundary conditions.

From general considerations it follows that such functions can be represented as a formal sum over elementary solutions of (1), e.g.,

$$\Psi(r, \theta) = \sum_{m=-\infty}^{\infty} C_m J_{|m|}(kr)\, \mathrm{e}^{\mathrm{i}m\theta}, \tag{2}$$

where $J_m(x)$ are usual Bessel functions and $C_{-m} = C_m^*$.

[1] Deceased.

The Berry conjecture signifies that for chaotic billiards such as the stadium billiard, real and imaginary parts of coefficients C_m with non-negative m are independent identically distributed Gaussian random variables with zero mean and variance computed from the normalization.

The beauty of this profound conjecture lies first of all in its simplicity and generality. On the other hand, it represents chaotic wavefunctions as completely structureless and 'uninteresting' objects which to some extent was the reason of relatively few investigations of the chaotic wavefunctions.

In 2002 Smilansky *et al* [2] stimulated a renewal of interest in this problem. Instead of considering the coefficients of an expansion as in (2) these authors looked for the nodal domains of wavefunctions, i.e. the regions where a function has a definite sign. They have also observed that for chaotic wavefunctions the nodal domains have a rich unexpected structure worth investigating in detail.

In [3] on physical grounds it was conjectured that the nodal domains of random wavefunctions (and, consequently, of chaotic wavefunctions) can be adequately described by a critical percolation model (see, e.g. [6]). Due to the universality of the critical percolation it is unessential what special percolation model is considered. All of them lead to the same critical exponents as well as to other universal quantities. In [3] it was checked numerically that many predictions of the critical percolation model, such as the number of connected domains, their area distribution, cluster fractal dimensions etc agree very well with corresponding quantities computed from the nodal domains of random (and chaotic) wavefunctions. In [4] it was demonstrated that the level domains (the regions where a function is bigger than a certain non-zero value) are well described by a non-critical percolation model. These and other investigations strongly suggest that the critical percolation model is applicable for the description of the nodal domains of random and chaotic wavefunctions. Though it sounds physically quite natural and can be confirmed by a careful application of Harris' criterion [4], a rigorous mathematical proof was not yet found and further numerical verifications are desirable.

The purpose of this paper is to check another prediction of the percolation model namely that the boundaries of the percolation clusters are described by what is called SLE_6 curves (see below). This statement was proved in 2001 for the critical percolation on the triangular lattice by Smirnov [7] and it is widely accepted that it remains true for all critical percolation models. For the nodal domains of random functions it leads to the conclusion that the nodal lines (curves where a function is zero) have to be also described by SLE_6 curves.

The plan of the paper is the following. In section 2 for completeness we give an informal introduction to the SLE curves. This name is attributed to two-dimensional self-avoiding curves generated by a one-dimensional Brownian motion with zero mean and the variance linear in time with a coefficient of proportionality equal to a real positive number κ. In 2000 Schramm proved that if a random self-avoiding curve is in a certain sense conformally invariant then it belongs to SLE curves with a certain value of κ. Smirnov's result [7] means that the percolation boundaries are generated by the Brownian motion with $\kappa = 6$. In section 3 we present the results of direct numerical calculations of corresponding Brownian-like generating curves for the nodal lines of random wavefunctions and found that they are well described by SLE_6. The inevitable drawback of numerical calculations is that one always deals with curves of finite size. But the theorem about the relation between the percolation boundaries and SLE_6 is valid only for infinite curves. To decrease such a finite size effect we use in section 4 a different version of SLE called dipolar SLE [10]. In this approach one first conformally transforms a given region into, say, an infinite band and then uses a suitably modified SLE equation. By this method we numerically demonstrate that the nodal lines

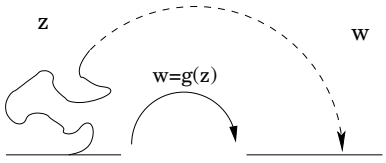

Figure 1. Loewner's evolution. The upper half plane of the variable z with a cutoff along a simple curve is transformed by a conformal map $w = g(z)$ to the whole upper half plane of the variable w. The tip of the curve is mapped to a real point ξ.

of random wavefunctions agree well with the SLE_6 description thus once more confirming the conjectural relation between the critical percolation and the nodal domains of random wavefunctions. In the appendix the numerical algorithms used in calculations are shortly discussed.

To a certain degree our work was stimulated by [5] where it was numerically checked that the nodal lines of the vorticity field in two-dimensional turbulence are close to SLE_6 curves. In the recent publication [11] Keating, Marklof and Williams have demonstrated that the nodal lines for a perturbed cat map are well described by SLE_6. They also performed [12] numerical calculations for the nodal lines of random wavefunctions which lead to the same conclusions. Our results are in complete agreement with their findings.

2. Schramm–Loewner evolution

The purpose of this section is to give a very informal discussion of SLE curves. For simplicity we stress in most cases only physical ideas. Precise mathematical definitions and profound theorems can be found, e.g., in review articles [13–16] and references therein.

Two-dimensional self-avoiding curves appear naturally in many physically important problems. But analytically imposing the condition of self-avoiding is not easy. In 1923 Loewner proposed [8] to describe such curves by conformal transformations which map a domain with a simple (i.e., without self-intersections) curve growing from the boundary to another domain without the curve. In the simplest setting one considers the upper half plane $\mathbb{H}$ with a simple curve $\mathcal{C}$ and looks for a conformal map which transforms the upper half plane minus the curve, $\mathbb{H}\backslash\mathcal{C}$, to $\mathbb{H}$ itself (see figure 1).

The main point of this approach is the well-known Riemann mapping theorem according to which any simply connected region (other than the whole plane and the plane without a point) can be conformally mapped to another simply connected region and, inversely, if one applies a conformal transformation to a simply connected region the result will be also a simply connected region.

Such conformal transformations are not unique and depend on three free parameters. For example, the upper half plane $\mathbb{H}$ is transformed to itself by a three-parameter group of fractional transformations

$$g(z) = \frac{az + b}{cz + d} \tag{3}$$

with real a, b, c, d.

To fix uniquely the conformal map $g(z)$ in situations as in figure 1 it is convenient to impose the so-called hydrodynamic normalization by fixing the behaviour of the map at infinity:

$$g(z) = z + \frac{2t}{z} + \cdots \quad \text{when} \quad |z| \to \infty. \tag{4}$$

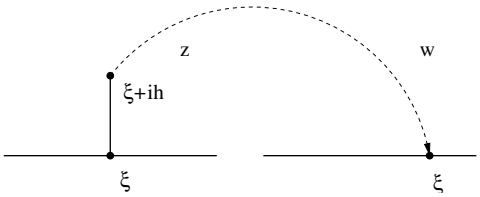

Figure 2. Transformation of a vertical slit to the upper half plane by map (6).

The coefficient $2t$ is a characteristic of the initial region called capacity (in $\mathbb{H}$ from infinity). For simplicity in what follow we refer to parameter t as to capacity omitting the traditional factor of 2. To stress its importance we shall denote the map $g(z)$ with asymptotic (4) by $g_t(z)$ showing explicitly the dependence of t.

Directly from (4) it follows that the capacity of successive application of two transformations with capacities s and t is the sum of these capacities. Loosely, it can be written as

$$g_t(g_s) = g_{t+s}. \tag{5}$$

This additive property deserves to call t 'conformal time' and permits to use the capacity to parametrize a growing curve.

The simplest example is a vertical slit growing in the upper half plane. If (ξ, h) are coordinates of the tip of the slit, $\gamma = \xi + \mathrm{i}h$ (see, figure 2) the transformation

$$w(z) = \xi + \sqrt{(z-\xi)^2 + 4t} \tag{6}$$

with $t = h^2/4$ maps the upper half plane of z with the slit to the upper half plane of w without the slit and $h = \sqrt{4t}$ is the equation of the growing slit parametrized by the capacity.

Interpreting t as the time permits to derive the Loewner equation for any simple growing curve (below we follow closely [15]).

Assume that γ_t denotes the tip of a simple curve starting from the real axis (γ_0 is real) and parametrized by its capacity, t. Let $g_t(z)$ be a conformal map which transforms the upper half plane minus this curve as in figure 1 to the upper half plane. In particular, it maps the tip of the curve to a real point $\xi_t = g_t(\gamma_t)$.

From (5) it follows that the evolution for time $t + \delta t$ can be considered as the evolution for the time t and then for a further short time δt

$$g_{t+\delta t}(z) = g_{\delta t}(g_t(z)). \tag{7}$$

For small δt any line can approximately be considered as a vertical slit growing from a real point ξ_t which is the image of the tip under $g_t(z)$ (cf appendix). Now (6) states that

$$g_{\delta t}(z) \overset{\delta t \to 0}{\longrightarrow} z + \frac{2\delta t}{z - \xi_t}. \tag{8}$$

Combining last two equations one concludes that $g_t(z)$ as a function of t obeys the following differential equation called Loewner's equation:

$$\frac{\mathrm{d}g_t(z)}{\mathrm{d}t} = \frac{2}{g_t(z) - \xi_t} \tag{9}$$

which has to be equipped with the initial condition

$$g_0(z) = z. \tag{10}$$

The function ξ_t is called the 'driving' or 'forcing' function. The curve itself is called the 'trace' and can formally be obtained from (cf [17, 18])

$$\gamma_t = g_t^{-1}(\xi_t). \tag{11}$$

The advantage of Loewner's equation (9) is that for any smooth (differentiable) function ξ_t it generates a two-dimensional self-avoiding curve.

The next important step was done by Schramm. In 2000 he proved [9] that two-dimensional random self-avoiding curves with conformal invariant measure (obeying certain technical conditions) are in Loewner's formalism generated by the one-dimensional Brownian motion with zero mean and the variance linear in t:

$$\xi_t = \sqrt{\kappa} B_t, \qquad \langle B_t \rangle = 0, \qquad \langle B_t B_s \rangle = \min(t, s). \tag{12}$$

Such curves only depend on one real positive parameter κ and are called stochastic (or Schramm) Loewner evolution curves or shortly SLE_κ curves.

As Brownian curves are not differentiable, SLE_κ curves may have self-touching points. Depending on the value of κ such curves are divided into three phases (see, e.g. [15]). For $0 < \kappa \leqslant 4$ the traces are simple curves, for $4 < \kappa < 8$ they can have double points or hit the real axis, and for $\kappa \geqslant 8$ they fill the entire domain.

SLE is a very powerful tool to study rigorously the scaling (continuum) limit of different discrete models (see [13–16]). The most important for us is the Smirnov's result [7]: the boundaries of clusters in the critical percolation (on a triangular lattice) converge in the continuum limit to the traces of SLE_6. As the nodal domains of random wavefunctions are conjectured to be described by critical percolation [3] it means that the nodal lines of random wavefunctions in this limit have to be also described by SLE_6 curves. The verification of this statement is the main purpose of this work.

3. The nodal lines of random wavefunctions

The nodal lines are the lines where a real function of two variables is zero, $\Psi(x, y) = 0$. They can, in principle, be computed numerically for any function $\Psi(x, y)$.

To calculate nodal lines for random wavefunctions (2) we proceed as follows (cf [3]). First one generates independent complex random coefficients C_m with the Gaussian distribution

$$P(C) = \frac{1}{2\pi} \exp(-|C|^2/2), \tag{13}$$

for $m = 0, \ldots, M_{\max}$ and put $C_{-m} = C_m^*$. The value of $M_{\max}$ is chosen of the order of kR where k is the momentum and R is the size of the region. Bessel function with $m > M_{\max}$ are small inside the region considered and can safely be neglected. For calculations below we choose the half-circular region with area equal 4π (i.e. $R = 2\sqrt{2}$) and $k = 100$. The region was divided into square lattice of the size $a = \lambda/30$ where $\lambda = 2\pi/k$ is the wavelength associated with k. Then for each realization of random coefficients one computes in all vertices of this lattice the sign of function (2).

As usual we consider nodal lines as a part of the dual lattice formed by straight lines passing through the middles of original edges which connect two vertices of opposite signs. Assume that function (2) is positive at the origin of the half-circle. We follow the real axis in the right direction till the first sign change is recorded. Then the nodal line grows along the dual lattice in such a way that the positive region remains always in the left. When a nodal line enters a square formed by four close-by vertices of the initial lattice this prescription determines uniquely in what direction it goes out.

For random wavefunctions (2) the nodal lines are quite complicated. An example of a nodal line is presented in figure 3. In this and similar pictures all distances are measured in the units of $1000a$ where $a = \lambda/30$ is the chosen lattice size. In these units the radius of the half-circle is $R = 3\sqrt{2}/\pi \approx 1.35$ for $k = 100$.

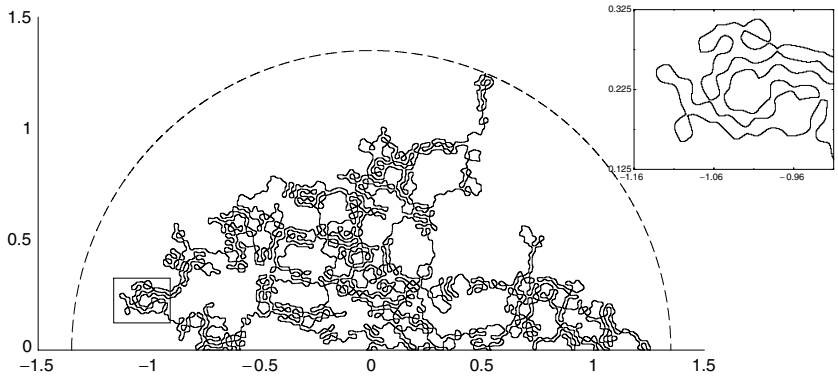

Figure 3. A nodal line of a random wavefunction. The dashed line indicates the absorbing half-circle. *Inset:* magnification of the indicated rectangular region.

To demonstrate the complexity and self-avoiding character of such a curve, its small portion enclosed by a rectangle is enlarged in the inset of this figure.

As all pictures of nodal lines are necessarily finite, one has to decide what to do when a nodal line hits the boundary. There are two main types of boundaries: reflecting and absorbing. If a growing line touches a reflecting boundary it follows the boundary in the increasing direction till the next appearance of the sign change and then continues along a new nodal line. This can be achieved automatically by imposing the sign of the function outside the boundary. If a boundary is absorbing, one simply stops any line which hits it. In figure 3 the horizontal line is a reflecting boundary but the half-circle indicated by the dashed line is an absorbing one. Different lines stop in different moments and have different number of points. The curve of figure 3 is one of the largest. It contains 65 150 points. Typical nodal line have near 18 000 points and we have computed approximately 2300 of them. To accelerate the calculations one may find the signs of random function (2) not at all lattice points but only locally in the vicinity of the growing nodal line.

In general, the properties of SLE_κ curves inside a region do depend on chosen boundary conditions. But for SLE_6 lines it is proved (see, e.g. [15]) that they have the so-called locality property, i.e., they feel the boundaries only when they hit them. So it seems that boundary conditions are unessential for the investigation of properties of the percolation cluster interfaces and, as conjectured, of the nodal lines of random wavefunctions. Nevertheless, we show in the next section that the statistical characteristics of the driving functions are sensitive to the choice of boundary conditions. The main point is that the standard Brownian description (12) is applicable only when all curves with 'time' t are taken into account. But one can argue that for any finite region there exist curves which during 'time' t go outside the region and return back. Boundary conditions will inevitably change these curves modifying their statistical properties.

Having generated a line as in figure 3, the next step is to find the conformal map which transforms it to the upper half plane. There are many good algorithms which permit us to do it numerically (see [19] and references therein). We used the so-called geodesic algorithm [19] in which a small segment of a line to be mapped is approximated by an arc of a geodesic circle perpendicular to the real axis and passing through the tip of the segment (see the appendix). This algorithm is quite stable and is easy to implement.

In figure 4 we plot the forcing function which corresponds to the nodal line of figure 3. Fine details of this function are given in figure 5. Note that, though nodal lines can be very

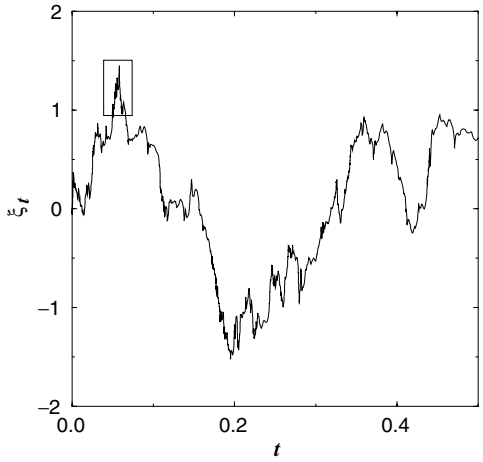

Figure 4. Forcing function corresponding to the nodal line of figure 3.

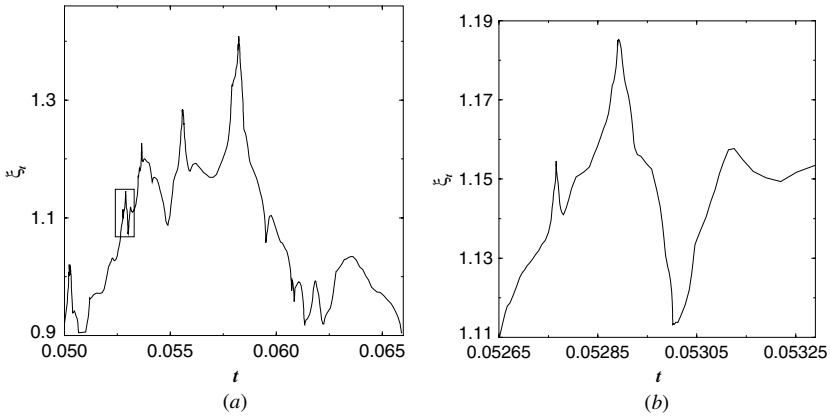

Figure 5. (*a*) Magnification of the small rectangular region in figure 4. (*b*) Magnification of the rectangular region in (*a*).

large (cf figure 3), their capacity (or maximal t for the forcing function) in the considered geometry is finite. It is the consequence of the general inequality for the capacity of a domain (a hull) (see, e.g. [14])

$$t < \tfrac{1}{2}R^2, \tag{14}$$

where R is the radius of the smallest half-circle centred on the real axis that contains the domain. In our case $R \approx 1.35$ and so for all curves $t < 0.91$.

We have numerically computed $N = 2248$ different realizations of the random wavefunction (2) with $k = 100$. For each realization we have found the nodal line starting from the origin and stopping when it hits the half-circle as in figure 3.

The corresponding forcing functions, $\xi_t(j)$ with $j = 1, \ldots, N$, were calculated using the geodesic algorithm. Nodal lines were computed with quite high precision of the order of $\lambda/30$. This was necessary to be sure that all complicated meanders of nodal lines are resolved. We check that to achieve an accuracy comparable with inevitable statistical errors (see below), calculations of forcing functions can be done using only $1/5$ of the total number of points

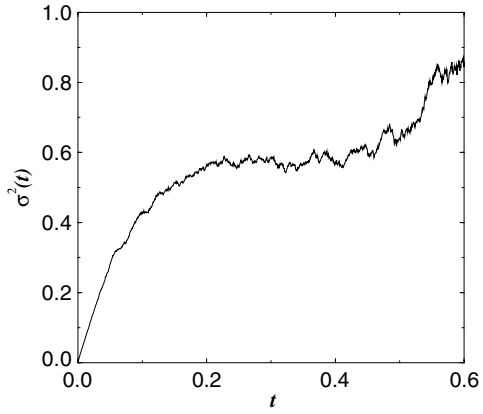

Figure 6. Variance of forcing functions for random waves inside the half-circle.

which considerably decreases the calculation time. So finally we calculate approximately 2300 different forcing functions and a typical function contains 3500 ± 100 points.

To compare these functions with Brownian curves predicted by SLE we calculated the mean value $\bar{\xi}_t$ and the variance $\sigma^2(t)$ for each t from the usual relations

$$\bar{\xi}_t = \frac{1}{N}\sum_{j=1}^{N} \xi_t(j), \qquad \sigma^2(t) = \frac{1}{N}\sum_{j=1}^{N} (\xi_t(j) - \bar{\xi}_t)^2. \tag{15}$$

According to the strict SLE_6 predictions (12) one should have $\bar{\xi} = 0$ and $\sigma^2 = 6t$. But for finite number of realizations of the Brownian motion curves one has statistical corrections to these values. In particular, one obtains the following estimates for the variance of SLE_κ within one standard deviation:

$$\sigma^2(t) \approx \left(\kappa \pm \kappa\sqrt{\frac{2}{N}}\right) t, \tag{16}$$

where N is the number of independent realizations. For the used value of N and $\kappa = 6$ it corresponds to 6 ± 0.18. Therefore, all obtained values of the slope in this interval do not contradict the SLE_6 prediction.

In figure 6 the calculated dependence $\sigma^2(t)$ is plotted versus t. It is clearly seen that contrary to the SLE expectation it is not linear. As we mentioned above this is not surprising as the linear behaviour is predicted only for infinite curves. Curves closed to boundaries which are absent in SLE (like the half-circle in figure 3) require a special treatment which we will discuss in the next section. For short time, when most of the curves do not feel the boundary, the variance is close to be linear.

In figure 7 the variance and the mean value are presented in a small interval of t where $\sigma^2(t)$ is approximately linear. The solid line in this figure is the best quadratic fit to the variance

$$y = -0.003 + 6.05t - 10.0t^2. \tag{17}$$

The most important for us is the value of the linear term, 6.05. It is quite close to the pure percolation value $\kappa = 6$. The mean value of the forcing functions (≈ 0) also agrees with the SLE value. Different fits to the data give slightly different values of coefficients. But in all cases the slope of the linear term is within the confidence interval 6 ± 0.18 (cf (16)) thus in accordance with SLE_6 expectation.

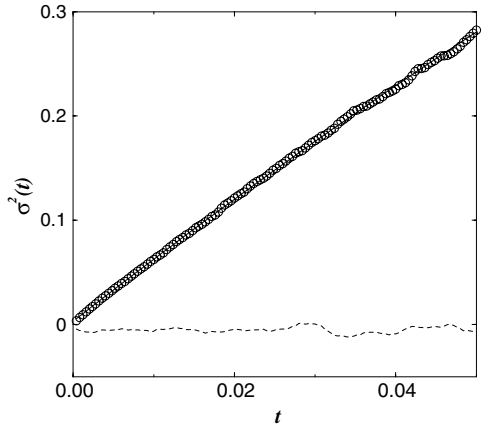

Figure 7. Variance (circles) and mean value (dashed line) in a short range. Solid line is the best quadratic fit (17).

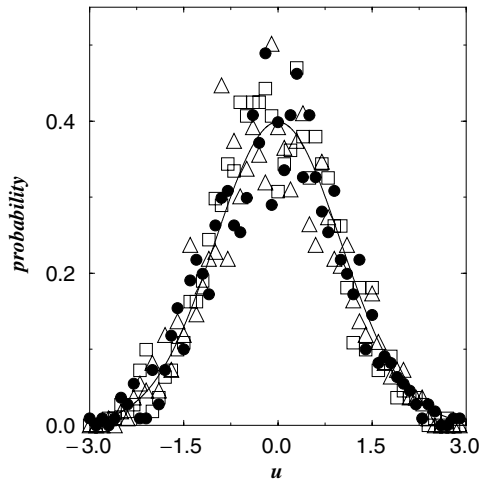

Figure 8. Probability law for random wave forcing functions. The abscissa axis is, as it follows for SLE_6, $u = \xi_t/\sqrt{6t}$. The solid line is the standard Gaussian $P(u) = e^{-u^2/2}/\sqrt{2\pi}$. The points indicated by ●, △ and □ correspond to, respectively, $t = 0.02$, 0.04 and 0.06.

Another important prediction of the SLE_6 description of the percolation model is that the distribution of values of ξ_t with fixed t has to be Gaussian with variance $6t$. In figure 8 this distribution is presented for different values of t. When the abscissa axis is rescaled by $\sqrt{6t}$ all data are quite close to the Gaussian curve with unit variance. Similar results were obtained when instead of the half-circle we consider nodal lines inside a rectangle.

The agreement of our results with SLE_6 predictions confirms that the nodal lines of random wavefunctions are well described by the percolation model, as was conjectured in [4].

4. Dipolar SLE

Though the results of the previous section are in a good agreement with SLE_6, let us notice two facts. First, the approximately linear increase of the variance with time is observed only

for a very small time interval. Second, even within this interval a quadratic term in t exists and is quite large (cf (17)). So, strictly speaking, the variance is a nonlinear function of t which contradicts the SLE. We have mentioned that these drawbacks are related with inevitable finite size effects. In this section we discuss this subject in more detail and show that both of them can be considerably reduced by using another variant of SLE.

First of all we note that there exist lines with arbitrary small capacity which can go arbitrarily far from the origin. The simplest way of seeing this phenomenon is to use the exact solution for the conformal map of the slit forming an angle $\pi\alpha$ with the real axis (see e.g. [18]). From this solution one concludes that for $\alpha \to 0\, t \to \alpha L^2/4$ where L is the length of the slit. Therefore straight lines with very small angle of inclination may go arbitrarily far for arbitrarily small time. Many lines close to the real axis also have this property.

The existence of such lines escaping very quickly demonstrates that for arbitrarily small time boundaries are important. Even for $t \to 0$ there are curves which go outside any finite region. These are the curves which will be modified by imposed boundary conditions.

This situation is quite analogous to the Brownian motion in a finite interval. It is well known (see e.g. [20]) that the probability for a one-dimensional Brownian particle starting from x_0 to arrive at the point x at time t in the whole space is given by the Green function of the diffusion equation

$$G_0(x, x_0; t) = \frac{1}{\sqrt{2\pi Dt}} \exp\left(-\frac{(x - x_0)^2}{2Dt}\right), \tag{18}$$

where D is a diffusion coefficient. Standard relations $\langle x\rangle = x_0$ and $\langle (x - x_0)^2\rangle = Dt$ which are analogue of (12) are simple consequences of this expression.

For the Brownian motion inside a finite interval the above probability depends on the boundary conditions. There are two main types of boundary conditions: reflecting and absorbing. When a particle hits a reflecting boundary it reflects back, when it touches an absorbing boundary it stops. It is known (see, e.g. [20]) within the formalism of the diffusion equation that a reflecting boundary gives rise to the Neumann boundary condition and an absorbing one corresponds to the Dirichlet condition. When both boundaries of an interval of length h are of the same type one gets that the Green function of this interval is

$$G_\pm(x, x_0; t) = \sum_{m=-\infty}^{\infty} (G_0(x + 2mh, x_0; t) \pm G_0(-x + (2m + 1)h, x_0; t)). \tag{19}$$

Here + (respectively −) denote Neumann (respectively Dirichlet) boundary conditions imposed at points $\pm h/2$.

In figure 9 the mean variance

$$\sigma^2(t) = \int_{-h/2}^{h/2} (x - \bar{x})^2 G_\pm(x, x_0; t)\, \mathrm{d}x \tag{20}$$

is plotted as a function of t for the case $x_0 = 0$ and $D = 1$. It is clearly seen that the long time behaviour is nonlinear and depends on the boundary conditions. The variance is linear in t only for very small t. It is the slope at the origin which corresponds to the true diffraction coefficient.

This figure is quite similar to figure 6 for the variance of forcing functions where the linear behaviour was observed only for very small $t < 0.05$ (cf figure 7). We estimated that in the best case this interval of t corresponds to, roughly speaking, only 1/4 of the total curve length. Even for this tiny interval the existence of a large quadratic term does not permit to perform the clear-cut comparison with SLE.

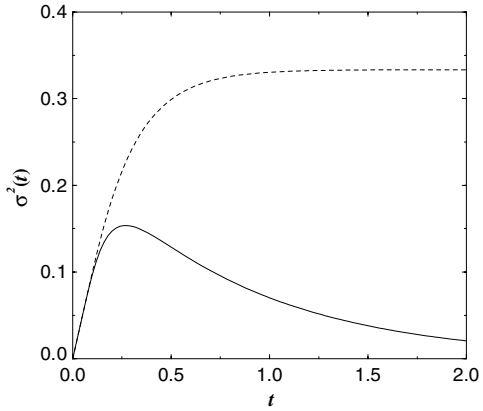

Figure 9. Variance for the one-dimensional Brownian motion with absorbing boundaries (solid line) and reflecting ones (dashed line).

To take into account larger parts of the curves and to check the linear Brownian-type behaviour for a longer time interval it is necessary to construct formulae similar to (19) for SLE.

The simplest case corresponds to the reflecting boundary conditions. In this setting one considers a region and random curves (nodal lines) which start at one fixed point, z_0, of the boundary and end at another fixed boundary point, z_1. For the nodal lines this can be achieved, e.g., by imposing that one boundary arc from z_0 to z_1 is positive and the other is negative. This type of processes is called chordal SLE (see, e.g. [15]). By definition, it can be reduced to the standard SLE from 0 to infinity (cf (9)) by a conformal transformation which transforms the given region to the upper half plane in such a way that the point z_0 is mapped to the origin and the point z_1 to infinity.

Here, we would like to use a different variant of SLE which corresponds to a region with two boundary arcs restricted by points z_+ and z_-. One arc is assumed to be a reflecting boundary and the other is an absorbing boundary. The random curves emerge from the point z_0 on the reflecting boundary and are stopped when they hit the absorbing arc. By a conformal transformation our region can be transformed to the standard strip $\mathbb{S}$,

$$\mathbb{S} = \{z \in \mathbb{C}, 0 < \operatorname{Im} z < \pi\}, \tag{21}$$

in such a way that points z_-, z_+ and z_0 are mapped to $-\infty$, $+\infty$ and 0, respectively.

In [10] it was shown that the SLE$_\kappa$ process which joins 0 to a point of the line $\operatorname{Im} z = \pi$ is described by the following Loewner-type equation:

$$\frac{\mathrm{d}g_t(z)}{\mathrm{d}t} = \frac{2}{\tanh(g_t(z) - \xi_t)}, \tag{22}$$

where $g_0(z) = z$ and the forcing function, ξ_t, is as above the standard Brownian motion (12) with variance κt.

To construct the dipolar SLE numerically from the data used in the previous section we first transform the nodal lines inside the half-circle, as in figure 3, to the standard strip (21) by the following transformation:

$$F(z) = \ln[(L + z)^2/(L - z)^2], \tag{23}$$

where L is the circle radius.

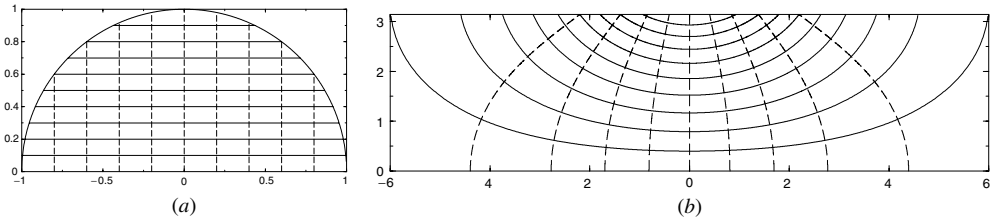

Figure 10. (*a*) Rectangular lattice inside the half-circle. (*b*) Its image under the map (23).

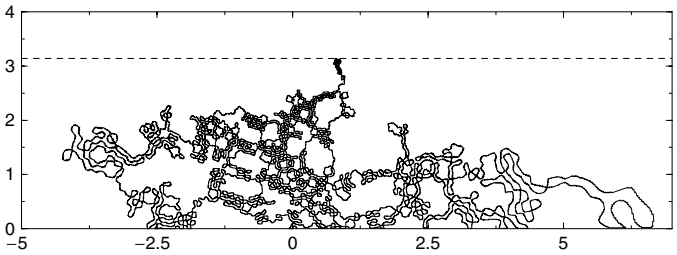

Figure 11. Image of the nodal line of figure 3 under the map (23). The dashed line is the absorbing boundary.

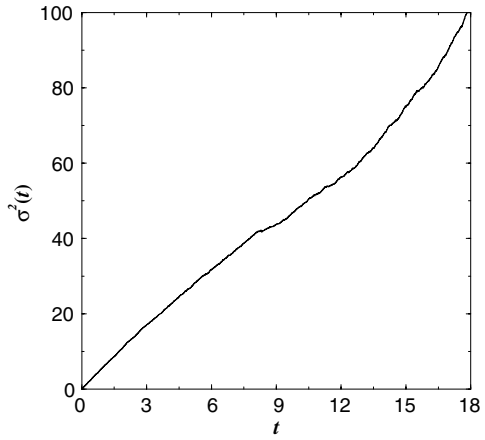

Figure 12. Variance of forcing functions for the nodal lines inside the strip.

To visualize this mapping we present the images of a rectangular lattice inside the half-circle in figure 10. Note the strong deformations of the regions close to the absorbing boundary.

The first step of calculations consists in the transformation of every nodal lines inside the half-circle to lines inside the chosen strip (21). Such an example is illustrated in figure 11.

Then it is necessary to find the dipolar conformal transformation which maps the strip with a line to the strip itself (cf (22)). In the appendix a simple algorithm for such a mapping is briefly discussed. Using it we compute numerically the forcing function, ξ_t for each nodal line and calculate its statistical properties. In figure 12 the variance (15) is plotted for all curves and in figure 13 the region of linear increase of $\sigma^2(t)$ is magnified. The solid line in this figure indicates the best quadratic fit

$$y = 5.92t - 0.103t^2. \tag{24}$$

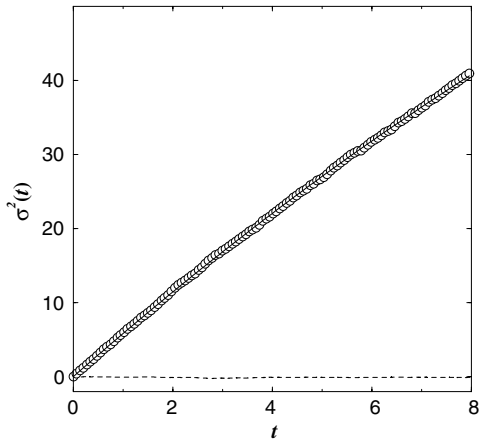

Figure 13. Variance (circles) and mean value (dashed line) for 2252 realizations inside the strip. Solid line: the best fit (24).

The coefficient 5.92 is to compare with the percolation theory value for this number of points: 6 ± 0.18. Different fits (with a constant term and (or) a cubic term) lead to the same conclusion. Other statistical characteristics are also in a good agreement with the SLE_6 predictions.

Contrary to (17) the quadratic term in (24) is small. We check that it is mainly related to discretization errors and it decreases when more points along a curve are taken into account. The nonlinear behaviour of the variance in figure 12 for large t is connected with large errors due to the stretching of lines close to the boundary as is obvious from figures 10 and 11.

The difference in scales in figure 7 for chordal SLE and in figure 13 for dipolar SLE is mostly related with different definition of 'time' in both approaches. Nevertheless, the interval $t < 8$ in figure 13 where the variance is linear in t is effectively much larger (i.e., contains more points of driving functions) than the corresponding interval $t < 0.05$ in figure 7. We have checked that the former includes approximately 92% of the typical curve length as compared to 25% for the latter. It means that the dipolar SLE_6 is a good description of the nodal lines practically for the entire nodal lines. Exceptions are small line parts close to the absorbing boundary which require better approximations.

We have also investigated nodal lines inside a rectangle $[-L/2; L/2] \times [0; l]$ which can be conformally mapped into the strip (21) by the following transformation

$$F(z) = -\ln[(\wp(z + L/2) - \wp(L))/(\wp(L/2) - \wp(L))], \tag{25}$$

where $\wp(z)$ is the Weierstrass elliptic function with periods $2L$ and $2il$ (see e.g. [21]).

The results in this case are similar to the ones above and all agree well with the percolation model.

5. Conclusions

In summary, we investigate the nodal lines of two-dimensional random wavefunctions by numerically computing one-dimensional forcing functions of Loewner's evolution. We demonstrate that the later are well described by a Brownian motion with zero mean and variance growing linearly in time. The coefficient of proportionality is close to the value 6 predicted by the percolation model. Our results give an additional support to the conjecture that the nodal domains of random wavefunctions in the scaling limit are described by the critical percolation.

We consider and compare the chordal and dipolar variants of SLE. In both cases the slopes of the variance are of comparable accuracy and within statistical incertanties are in agreement with SLE_6. But for the dipolar case the interval where the variance is linear in time is not only considerably larger than for the chordal one but also all nonlinear terms are practically absent, which is not the case for the chordal SLE. It demonstrates that using the dipolar SLE reduces significantly finite size effects.

Acknowledgments

The authors are very thankful to J Keating and I Williams for useful discussions and, in particular, for pointing out an error in the calculations. One of the authors, EB, is grateful to G Falkovich for the discussion of the paper [5] prior the publication and to D Bernard for clarifying discussions about SLE.

Appendix

Consider a simple curve which starts on the real axis and grows inside a region of the upper half plane. The goal of the numerical algorithms below is to find a forcing function in (9) corresponding to a conformal map which transforms the region cut along the curve into the region itself.

Let $(x_0, 0)$ be coordinates of the first point of the curve which we assume belongs to the abscissa axis and let (x_1, y_1) be coordinates of the next point closest to the first. The simplest numerical method consists of assuming that the forcing function is a piecewise constant function. The map with a constant forcing function $\delta\xi$ for $0 < t \leqslant \delta t$ is given by (6) as

$$g_t(z) = \delta\xi + \sqrt{(z-\delta\xi)^2 + 4\delta t}. \tag{A.1}$$

The parameters $\delta\xi$ and δt are obtained from the condition that the top of the slit coincides with the point $\delta z = x_1 - x_0 + \mathrm{i}y_1$, which yields

$$\delta\xi = \mathrm{Re}\,\delta z, \qquad \delta t = \tfrac{1}{4}(\mathrm{Im}\,\delta z)^2. \tag{A.2}$$

Then we transform all points of the curve except the first one by (A.1) with these values of parameters and renumber the resulting points. One repeats this process till the whole curve will be transformed. In [17] it is proved that such an algorithm converges for sufficiently small δt_j and δx_j.

In section 3 we used the more refined geodesic algorithm [19] in which one approximates a small part of the curve between two points, 0 and δz, by the geodesic arc (a circle perpendicular to the real axis) passing through these points. Normalizing the map given in [19] such as to obey the convention (4) one gets the expression

$$g_t(z) = \frac{b^3}{\sqrt{b^2+c^2}\sqrt{(bz/(b-z))^2+c^2} - b^2 - c^2} + \frac{2b^3+3bc^2}{2(b^2+c^2)}, \tag{A.3}$$

where

$$b = \frac{|\delta z|^2}{\mathrm{Re}\,\delta z}, \qquad c = \frac{|\delta z|^2}{\mathrm{Im}\,\delta z}. \tag{A.4}$$

Direct calculations give that the time corresponding to δz and the value of the forcing function in this point are

$$\delta t = \tfrac{1}{4}(\mathrm{Im}\,\delta z)^2 + \tfrac{1}{8}(\mathrm{Re}\,\delta z)^2 \tag{A.5}$$

and

$$\delta\xi_t = \tfrac{3}{2}\,\mathrm{Re}\,\delta z. \tag{A.6}$$

When a point moves along a geodesic circle of diameter b the forcing function changes as follows:

$$\xi_t = \frac{12t}{b + \sqrt{b^2 - 8t}} \tag{A.7}$$

and is practically linear for short time. Equations (A.3)–(A.6) define the geodesic algorithm.

To do some computations following dipolar SLE in section 4 we use a piecewise constant approximation for the forcing function in (22). In this case one has the exact solution [10]

$$\cosh\left(\tfrac{1}{2}(g_t(z) - \delta\xi)\right) = \mathrm{e}^{\delta t/2}\cosh\left(\tfrac{1}{2}(z - \delta\xi)\right). \tag{A.8}$$

Finding δt and $\delta\xi$ from the condition that the curve tip coincides with δz one obtains

$$\delta\xi = \mathrm{Re}\,\delta z, \qquad \exp\left(-\tfrac{1}{2}\delta t\right) = \cos\left(\tfrac{1}{2}\,\mathrm{Im}\,\delta z\right). \tag{A.9}$$

These expressions are the dipolar analogue of equations (A.2) and they permit to construct the simplest algorithm of numerical calculations for the dipolar case.

References

[1] Berry M V 1977 Regular and irregular semi-classical wavefunctions *J. Phys. A: Math. Gen.* **10** 2083
[2] Blum G, Gnutzmann S and Smilansky U 2002 Nodal domains statistics: a criterion for quantum chaos *Phys. Rev. Lett.* **88** 114101
[3] Bogomolny E and Schmit C 2002 Percolation model for nodal domains of chaotic wave functions *Phys. Rev. Lett.* **88** 114102
[4] Bogomolny E and Schmit C 2006 Random wave functions and percolation (in preparation)
[5] Bernard D, Boffetta G, Celani A and Falkovich G 2006 Conformal invariance in turbulence *Nature* **2** 124
[6] Stauffer D and Aharony A 1994 *Introduction to Percolation Theory* (London: Taylor and Fransis)
[7] Smirnov S 2001 Critical percolation in the plane : conformal invariance, Cardy's formula, scaling limits *Acad. Sci., Paris* I **333** 239
[8] Löwner K 1923 Untersuchungen über schlichte konforme Abbildungen des Einheitskreises I *Math. Ann.* **89** 103
[9] Schramm O 2000 Scaling limits of loops-erased random walks and uniform spanning trees *Isr. J. Math.* **118** 221
[10] Bauer M, Bernard D and Houdayer J 2005 Dipolar stochastic Loewner evolution *J. Stat. Mech.* P03001
[11] Keating J P, Marklof J and Williams I G 2006 Nodal domain statistics for quantum maps, percolation and stochastic Loewner evolution *Phys. Rev. Lett.* **97** 034101
[12] Keating J P and Williams I G 2006 private communication
[13] Lawler G F 2001 An introduction to the stochastic Loewner evolution *Proceedings of Conference on Random Walks* (Vienna: Erwin Schrodinger Institute)
[14] Kager W and Nienhuis B 2004 A guide to stochastic Löwner evolution and its applications *J. Stat. Phys.* **115** 1149
[15] Cardy J 2005 SLE for theoretical physicists *Ann. Phys.* **318** 81
[16] Werner W 2004 *Random Planar Curves and Schramm–Loewner Evolution* (*Lectures Notes in Mathematics* vol 1840) p 107
[17] Bauer R O 2003 Discrete Loewner evolution (*Preprint* math.PR/0303119)
[18] Kennedy T 2005 A fast algorithm for simulating the chordal Schramm–Loewner evolution (*Preprint* math.PR/0508002)
[19] Marshall D and Rohde S 2005 Convergence of the Zipper algorithm for conformal mapping http://www.math.washington.edu/~marshall/preprints/zipper.pdf
[20] Feller W 1968 *An Introduction to Probability Theory and its Applications* (New York: Wiley)
[21] Erdélyi A 1955 *Higher Transcendental Functions* vol 3 (New York: Mc Graw-Hill)